Materials Science-Poland, 41(1), 2023, pp. 94-109
http://www.materialsscience.pwr.wroc.pl/
DOI: 10.2478/msp-2023-0011

sciendo

Evaluation of the possibility of improving the durability of tools made of X153CrMoV12 steel used in the extrusion of a clay band in ceramic roof tile production

Marek Hawryluk[1,*], Jan Marzec[1,2], Marzena Lachowicz[1], Piotr Makuła[1], Kamila Nowak[1]

[1]Wroclaw University of Science and Technology, Wroclaw, Poland
[2]Röben Polska, Środa Śląska, Poland

The article presents the results of a complex comparative analysis of the abrasive wear resistance of tools made of X153CrMoV12 steel after different heat treatment variants. These investigations aimed to select the most durable material for application in tools forming a mass band in the production of ceramic roof tiles. The tests included the determination of resistance to abrasive wear in ball-on-disc tests, hardness measurements, and microstructure analysis, including the assessment of changes occurring in the subsurface area, as well as impact tests (at a working temperature for the tools of 50°C). The comprehensive test results showed that the best effects of increasing the resistance to abrasive wear can be obtained through a heat treatment that consists of hardening at 1020°C and then tempering at 200°C for about 2 hours. The next stage of research will be to compare the results obtained with another popular material for tools for the production of roof tiles – Hardox steel, which is characterized by high resistance to abrasive wear.

Keywords: *roof tiles, tribological wear, ball-on-disc test, impact tests, increase wear resistance, microstructure*

1. Introduction

Currently, one main focus of the development of machine construction is the optimization of machine parts in terms of their resistance to abrasive wear. The phenomenon of intensive abrasive wear is encountered in many branches of industry, most prominently the extractive, concrete, ceramic, and metallurgical industries [1, 2]. Abrasion is also a very important consideration during the performance of machines and devices for earthworks, which applied in agriculture and construction [3, 4]. Additionally, because of progress in the development of environmental protection, much research is conducted with the aim of prolonging the operation time of machines in direct contact with the materials used in waste recycling, e.g., metal shredder blades, transportation containers, and so forth. [5]. Excessive wear of machine parts negatively affects the entire production and technological process. An especially aggressive working environment is encountered in the ceramics industry, particularly on roof tile production lines, where key machine elements regularly come into direct contact with the processed material, whose main components are clay, quartz sand, and ground crushed brick [6]. The most intensive abrasion occurs in the process of band extrusion, where the production mass is mixed, homogenized, vented, and formed [7]. This process is currently realized in horizontal band plungers, which are made up of a two-shaft mixer and a pug mill [8, 9]. The production mass processed by these machines is at a humidity level of 20%–25% and is compressed in the pug mill head under 2–10 MPa of pressure. The product at this stage of production is an extruded band that is formed by a set of two special tools (plates) which are exposed to especially intensive abrasive wear and an increase in working temperature [10]. This is the effect of the direct contact of the tool with the processed material and the high pressure exerted during the band extrusion. The working conditions present in the band extrusion process require the application of materials resistant to abrasion, which make it possible to prolong the per-

* E-mail: marek.hawryluk@pwr.edu.pl

© Hawryluk et al. 2023. This is an open access article distributed under the Creative Commons Attribution-NonCommercial-NoDerivatives 4.0 License. (http://creativecommons.org/licenses/by-nc-nd/4.0/)

formance life of the machine parts. Currently, the tools forming the clay band in the production of ceramic roof tiles are more and more often made of cold work high-chromium tool steels. These materials have so far been widely applied as materials for machining tools and tools for plastic formation, especially formation of metal sheets in the processes of die shearing and pressing. From the performance tests conducted so far for the ceramic industry, we can conclude that the application of NC11LV steel after the classic heat treatment for tools forming the band prolongs their operation time by almost 60% with tools made of Hardox 600 steel [11, 12]. The most commonly used cold work high alloy tool steels include X165CrV12 (NC10), X210Cr12 (NC11), and X153CrMoV12 (NC11LV) [13]. The nominal carbon content in the case of the first two equals 1.65% (NC10) and 2.1% (NC11), respectively. Steel NC11LV characteristically has a slightly lower carbon content and a similar chromium content compared to that of steel NC10. It is distinguished by the presence of alloy additions, such as molybdenum and vanadium (about 1%) [14, 15]. Tool steels owe their high abrasive wear resistance and good working parameters mostly to their high (10%–15%) chromium content. The high chromium content increases its hardenability. It also increases the austenitization temperature and the kinetics of the phase transformations taking place during cooling in the hardening process. In the case of cold work tool steels, it is possible to harden tools with any dimensions at different cooling rates. The microstructure of these materials, apart from a martensitic matrix, is also formed by carbides, mainly of the M_7C_3 type [16]. The size, shape, and distribution of the carbides play an important role in the process of friction and the subsequent material wear. Additionally, the carbides present in NC11LV steel, as a result of prolonged annealing, can undergo transformation from M_7C_3 carbides into $M_{23}C_6$ carbides. The transformation takes place at high temperatures owing to iron's diffusion into the matrix and that of chromium—from the matrix into the peripheral regions [17, 18]. All these characteristics enable a high level of control of the heat treatment process in high chromium tool steels. The basic surface engineering method improving the mechanical properties of cold work tool steels is thermochemical treatment, mainly nitriding, which makes it possible to increase the hardness and improve the abrasive wear resistance in the area of the surface layer [19]. Nitriding of high chromium tool steels is realized in two ways, i.e., using ion or gas [20]. The most important parameters of the whole process determining the thickness of the nitrided layer are the nitriding temperature and time. In the case of NC11LV steel, the nitrided layer's thickness depends largely on the matrix structure of the hardened material. This is caused by the fact that, in austenite, the nitrogen diffusion runs more slowly than in martensite. Owing to the properties of high chromium tool steels, especially steel NC11LV, they are a good alternative for the abrasion-resistant Hardox steels [21]. In order to precisely determine the material's abrasion wear resistance, many advanced studies are currently being conducted. The most prevalent include examinations with dry abradants, as well as the roll-on-block, pin-on-disc, and ball-on-disc tests [22–24].

As was pointed out above, the performance tests conducted so far confirm the effectiveness of the use of NC11LV steel for tools forming the clay band in ceramic roof tile production. In this analysis, the material was subjected to classic heat treatment, i.e., hardening combined with low temper-

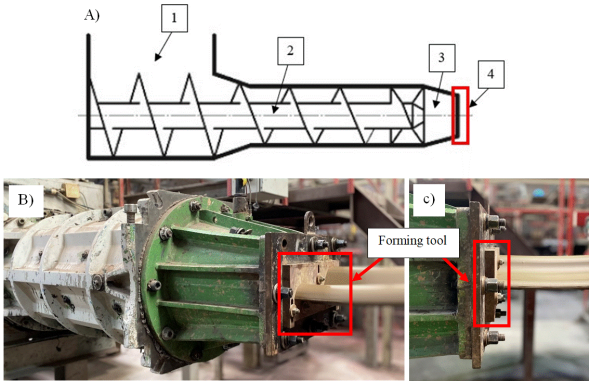


Fig. 1. Ceramic roof tile extrusion process – A) schematic diagram of construction of extruder barrels: 1 - vacuum zone, 2 - screw, 3 - pressure head, 4 - forming tool [25], B) main view of extruder, C) process of band forming

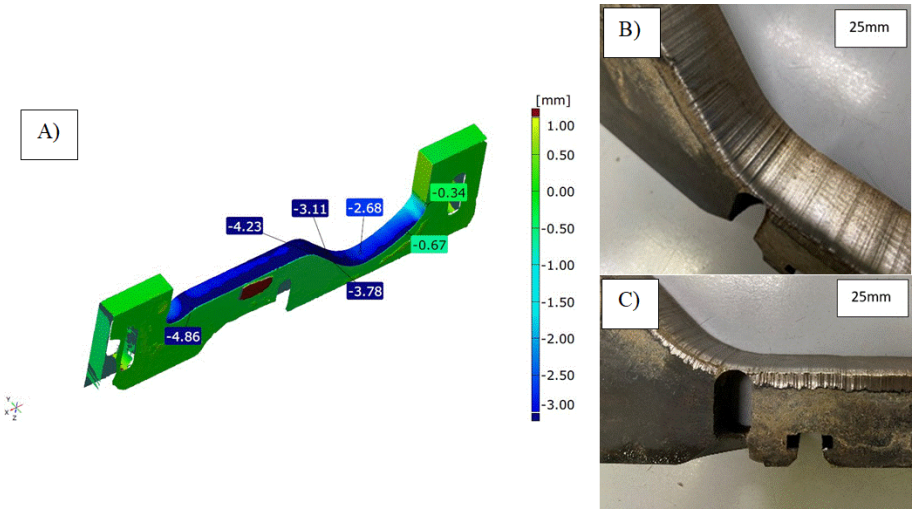


Fig. 2. Example of worn tool – A) results of 3D scanning, B) scratches, C) crack

ing. This causes the low ductility characteristic of some tool steels. In the case of tools that form the band, this can lead, in critical cases, to cracking in the notch area, which is formed as a result of deep scratches on the working surface. Therefore, it is advisable to improve the plastic properties. Taking this into account, the study performs a complex comparative analysis of approaches to forming the properties of NC11LV tool steel by means of heat treatment. The aim of the modification of the heat treatment parameters was to obtain higher ductility while maintaining the high hardness value, as the optimal material characteristics for tools forming the clay band in ceramic roof tile production.

2. Materials and methods

The basic tool (plate) used in the forming the clay band in the process of producing ceramic roof tiles was chosen for the heat treatment analysis (see Figure 1). This tool is used at the forming stage and is responsible for preliminarily shaping the tile during the mass band extrusion in the pug mill. In the first stage of the extrusion process, the production mass is vented in the vacuum zone, then it is transported by a screw conveyor to a pressure head. Finally, the production mass is compressed, formed, and extruded under a pressure of 20 MPa. Next, the band prepared in this way is cut into a specific size and finally formed on a punch press. The plates are very important elements as the degree and type of wear affect the quality of the final product. During operation, these tools are exposed to intensive abrasive wear due to their direct contact with the processed material.

The tool is used until critical wear is reached, which makes it impossible to adjust the thickness of the band. The critical defect of the forming tools is deep scratches that affect the quality of the final product. Most of the damage is the result of abrasive wear caused by hard particles, whose presence is an effect of adding milled remains of burned-out tiles to the production mass. An example of a worn tool and photos of typical damage to the work surface are shown in Figure 2.

For the tests performed, cold work tool steel X153CrMoV12 was used, which is also known under the denotation NC11LV. Its chemical composition is provided in Table 1. The chemical composition was tested using the glow discharge optical emission Spectrometry (GD OES) method. The Leco GDS 500A analyzer was used.

In the tests conducted, NC11LV steel was subjected to three variants of additional heat treatment. The applied heat treatment variants for the particular samples are provided in Table 2. The parameters were selected in order to check how the mechanical properties of the chosen steel grade, especially its

Table 1. Chemical composition of X153CrMoV12 steel

Steel X153CrMoV12 (NC11LV) – chemical composition [%]											
C	**Si**	**Mn**	**P**	**S**	**Cr**	**Mo**	**Ni**	**Al**	**Cu**	**V**	**W**
1.59	0.25	0.38	0.012	0.008	11.72	0.88	0.20	0.03	0.06	0.76	0.05

Table 2. Parameters of the test samples' heat treatment

Sample no.	Austenitizing temperature [°C]	Tempering temperature [°C]	Tempering time [h]
960/450	960	450	2
1060/450	1060	450	2
1020/200	1020	200	2

impact strength, would change. Hardness is one of the parameters that provide resistance to abrasion. For this reason, optimally high hardness that is as constant as possible is used in tool steels. However, the ductility remains quite low, which increases susceptibility to tool cracks. The applied tempering temperature of 450°C should make it possible to maintain high hardness, at the same time improving the ductility. For an additional verification of the heat treatment parameters, two austenitization temperatures were selected, i.e., 960°C and 1060°C. The reference point for the conducted tests was a sample subjected to classic heat treatment, that is quenched at 1020°C followed by tempering at 200°C.

In order to perform a complex analysis, the following tests were conducted:

- Examination of the selected mechanical properties: the micro-hardness and the impact strength.
- Examination of the impact strength: performed on samples with a V notch made according to the norm EN 10045-1, on a Charpy hammer at 50°C and 200°C.
- A ball-on-disc test conducted on a tribological tester DUCOM of the ball-disc type in order to estimate the tribological properties under conditions of dry friction for a pair: Al_2O_3 ball–NC11LV steel disc (test samples), with a load of 10 N, path of 300 m, and rubbing speed of 0.1 m/s.
- A microstructure test: performed by means of a metallographic microscope by Leica, model DM6000M, and a scanning electron microscope Phenom Pro X after etching in 2% Nital.
- A topography analysis: for a SEM analysis of the tool surface, with the use of a scanning electron microscope Tescan Vega 3 with a BSE detector, with a voltage of 30 kV and magnification of up to 1 million times.

3. Research and discussion

3.1. Examinations of selected mechanical properties: hardness and impact strength

Within the investigations of the mechanical properties, hardness measurements of three samples were conducted. The measurement results have been collected and presented in Figure 3. The hardness of sample 960/450 equaled 485 ± 7

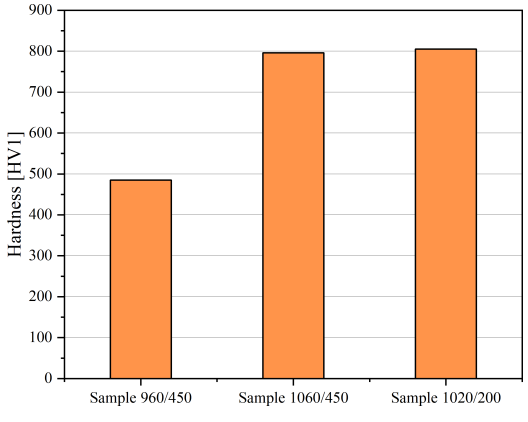


Fig. 3. Results of hardness measurements of steel after the performed heat treatment variants

Table 3. Results of the impact energy of samples with a V-notch

Material	Sample no.	Test temperature	Energy
		°C	J
NC11LV	960/450	50	3.8
	1060/450	50	3.7
	1020/200	50	2.8
	960/450	200	4.9
	1060/450	200	4.6
	1020/200	200	3.1
Hardox 600	1	50	21.6
	2	200	24.3

HV1 (≈ 48 HRC). Also determined was the material hardness in the matrix areas devoid of large primary carbide precipitations, which equaled 414 ± 23 HV0.1 (≈ 41 HRC). For sample 1060/450, the hardness of steel NC11LV after the applied heat treatment equaled much less, i.e., 796 ± 10 HV1 (≈ 64 HRC), whereas the hardness of the matrix was 598 ± 28 HV0.1 (≈ 55 HRC). Sample 1020/200 (cut out of the material of the tool [plate]) was also characterized at very high level of hardness—about 805 HV1 ± 14 HV1 (≈ 65 HRC), with the matrix hardness reaching 700 HV1 (≈ 61 HRC). A higher matrix hardness after the classic heat treatment results from a lower degree of martensite decomposition. Clear differences were, in turn, observed in the case of the matrix of the material tempered at the same temperature but with a different austenitization temperature. This should be connected with a different degree of saturation by the alloy elements. In comparison, the commercial wear-resistant Hardox 600 steel, commonly used for machine parts in the ceramics industry, demonstrates hardness at the level of 590 HV1.

The impact strength was also determined in these studies. The Charpy V-notch values (CVN) obtained have been collected and are presented in Table 3. The results for tool steel NC11LV are presented in comparison with the results for wear-resistant steel Hardox 600. For all the samples, the impact strength measurement was conducted at two temperatures, 50°C and 200°C, where the first value corresponded to the working temperature of the tool under industrial conditions, and the second value corresponded to the extreme temperatures present in the process of producing ceramic roof tiles during drying.

As we can observe, tool steel NC11LV under different states of heat treatment, the impact strength undergoes a slight change. Only in the case of sample 1020/200 can we see that the CVN coefficient is minimally lower than in the case of the other two samples, and it equals 2.8 J at the working temperature. We can conclude from the tests performed that the impact strength of steel NC11LV demonstrates stability at 200°C.

The impact strength test results unequivocally show that tool steel NC11LV hardened to the value of about 60 HRC (hardness Rockwell C) exhibits low ductility, which can favor a tendency for cracking. This is caused mainly by the presence in the structure of hard and undeformable carbides, which lower the hardness of tool steel NC11LV and at the same time significantly lower its impact strength.

As a comparison of the crack resistance of wear-resistant materials, Table 3 also includes steel Hardox 600. This steel is characterized by an impact energy equaling 21.6 J. In the case of application for plates forming a clay band, no large risk exists for critical impact loads of the examined steel NC11LV. In extreme cases, there is, however, a possibility of the plate's breaking in the area of the notch, which is formed as a result of deep scratches in the working surfaces. Examples of such damage to the tool made of NC11LV are shown in Figure 4.

In most cases, the forming tools are exposed to mostly continuous loads resulting from the pressure of the extruded mass onto the working surface of the plate.

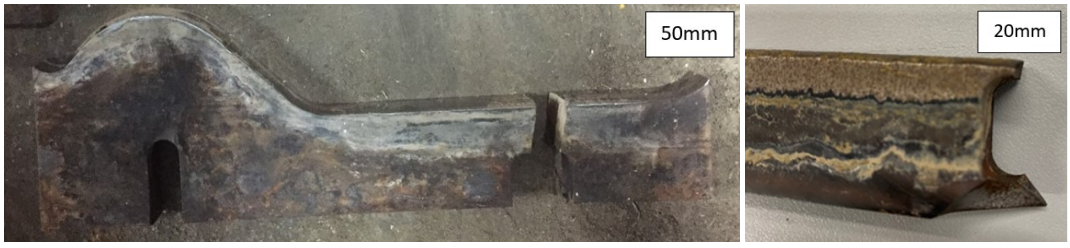


Fig. 4. Examples of damage in the form of cracks to the NC11LV tools forming the clay band

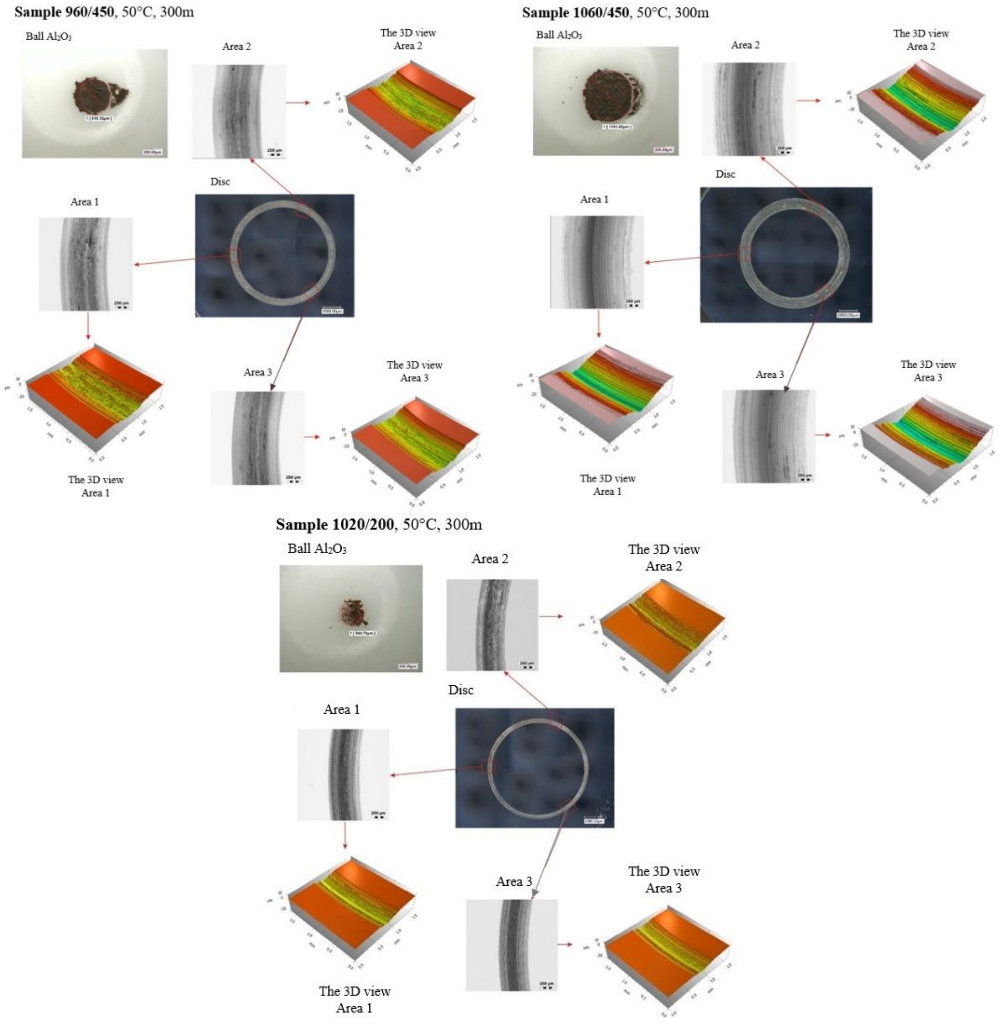


Fig. 5. Results of the ball-on-disc tests for the analyzed materials

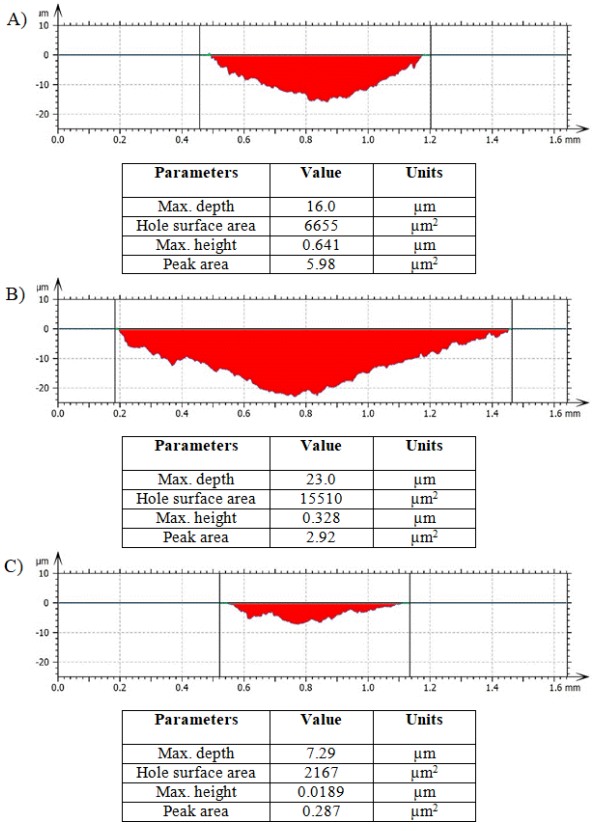
3.2. Ball-on-disc test

In the analysis of the abrasive wear of NC11LV steel, the material loss was determined based on the traces of wear obtained in the conducted ball-on-disc test. An Al_2O_3 ball was used as the clamp element. The test temperature was assumed to be 50°C, which was in agreement with the actual temperature present on the clay band-tool contact in the band extrusion process during the production of ceramic roof tiles. Figure 5 presents the test results for NC11LV steel in three heat treatment vari-

ants. The results presented illustrate the effects of the ball-on-disc test on the length of 300 m together with the magnified three-track areas. We can observe that the highest wear occurs for sample 1060/450, which was quenched at 1060°C and tempered at 450°C. The mean depth of the wear tracks for this sample equals 22.8 µm. Slightly better results were obtained in the case of sample 960/450, which was quenched from a lower temperature (960°C) and also tempered at 450°C. The averaged depth of the wear track from the three examined areas for sample 960/450 equals 13.7 µm. The lowest wear in the ball-on-disc test is exhibited by sample 1020/200 after the classic heat treatment. In the case of sample 1020/200, the mean track depth is at the level of 6.7 µm. The cause of the highest wear of sample 1060/450 is the presence of numerous spallings, which were observed by means of further microscopic observations. The spallings were created especially in the presence of primary carbides. The effect of this is excessive material wear caused by spalling of the material, which, at further stages, constitutes an abradant, contributing to intensification of the abrasion wear. The effect of the carbide particles' spallings on the increase of wear has also been confirmed by other authors [26].

In the analyzed areas of all the samples examined, we can see different levels of wear. This is connected with a non-uniform distribution of the carbide precipitates, which, in the friction process, undergo spalling in a random manner.

Figure 6 presents the track profiles obtained during the ball-on-disc tests for the materials analyzed. On the profiles, we can clearly see differences in the track depths. The track depth for sample 1020/200 is almost three times smaller than in the case of sample 1060/450 and nearly twice as low as for sample 1060/450. Large discrepancies can be seen in the case of the track widths. The track width of the sample that had worn the most is over twice as high as that in the other cases. The highest track width of sample 1060/450 additionally confirms that, in the case of this sample, material spalling took place in the extreme areas of contact between the ball and the steel disk, which intensified the material wear. Phenomena leading to the formation of numerous spallings on the surface of this sample were also observed in the microscopic tests, which are presented in subsequent sections of the article.



Parameters	Value	Units
Max. depth	16.0	µm
Hole surface area	6655	µm²
Max. height	0.641	µm
Peak area	5.98	µm²

Parameters	Value	Units
Max. depth	23.0	µm
Hole surface area	15510	µm²
Max. height	0.328	µm
Peak area	2.92	µm²

Parameters	Value	Units
Max. depth	7.29	µm
Hole surface area	2167	µm²
Max. height	0.0189	µm
Peak area	0.287	µm²

Fig. 6. Track profiles for the ball-on-disc test: A) sample 960/450, B) sample 1060/450, C) sample 1020/200

The most important parameters obtained in the ball-on-disc test for the analyzed materials have been compiled in Table 4. This illustrates the big differences between the wear of the particular samples.

Table 4. Results of the measurement of the track volume in the ball-on-disc test

Parameters	Sample 960/450	Sample 1060/450	Sample 1020/200
Track volume	9622503	20987030	3397096
Max. track depth	17.0	21.7	7.46

In ball-on-disc test, the values of the friction coefficient were also determined from the test for the whole measurement line 300 m, shown in Figure 7.

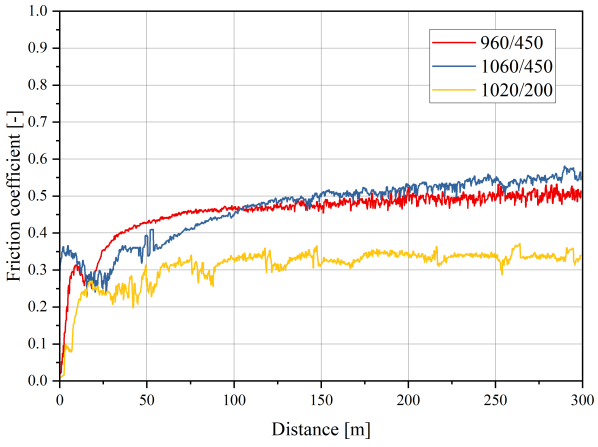


Fig. 7. Friction coefficients in the ball-on-disc test for both analyzed materials

On the basis of the obtained friction coefficient courses, we can observe some differences between the sample that underwent the smallest wear and the other two samples. The friction coefficient values for samples 960/450 and 1060/450 in the initial phase have a tendency to increase, and stabilization of the values can be seen after 100 m. The final value of the friction coefficient for these samples stabilizes within a range of 0.5–0.55. In the case of sample 1020/200, we can also see, just like at the first stage of the ball-on-disc test, that the friction coefficient increases for the first 50 m, and next oscillates around 0.35.

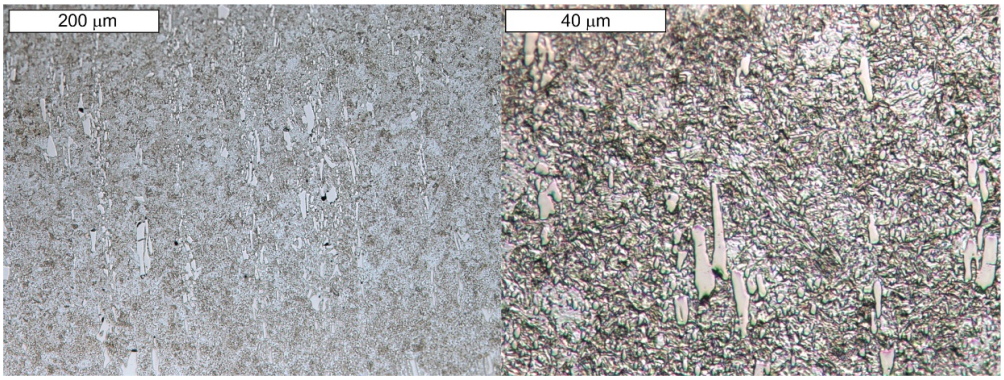
3.3. Tests of the material microstructure after different heat treatment variants

Figure 8 presents the microstructure of steel for sample 960/450. The samples for the microscopic tests were collected from the material's core. The microstructure of the material examined was constituted of precipitates of primary carbides type M_7C_3, elongated in the direction of plastic deformation in the martensitic matrix. For an additional identification of the phases formed in the microstructure of steel NC11LV, element distributions with the EDS method were carried out for the examined area of sample 960/450. The results of this analysis have been presented in Figure 9. The element distribution obtained for the tested material shows that the chemical composition of the carbides includes chromium or vanadium. The presence of chromium in the precipitates excludes the possibility of the formation of the interstitial carbides with a simple, closed-packet structure: MC and M_2C type, which demonstrate very good melting points. The co-existence of chromium and vanadium points to the formation of the interstitial carbides with a complex hexagonal, close-packed structure of the M_7C_3 type. In this case, vanadium, similarly to molybdenum, replaces the chromium atoms, forming a multi-component carbide $(Cr,V,Mo)_7C_3$. It was established that even a 4% addition of vanadium affects the type of the formed carbide. At the same time, no presence of separate MC carbides was observed [27]. Analytical tests were performed for the other samples, obtaining similar element distributions.

The microstructure of sample 1060/450 showed a similar character (Figure 10). A difference can be noticed in the form of tempered martensite, which, in this case, has a more crypto-acicular character. It was observed in the microscopic examinations that, together with the application of a higher austenitizing temperature (1060°C), the number of carbides was significantly lower compared to the other samples, which were quenched from lower temperatures. In the case of sample 1020/200 (Figure 11), the matrix was constituted of low-temperature-tempered martensite. In its background, one could observe primary carbide precipitates elongated in the direction of plastic deformation.

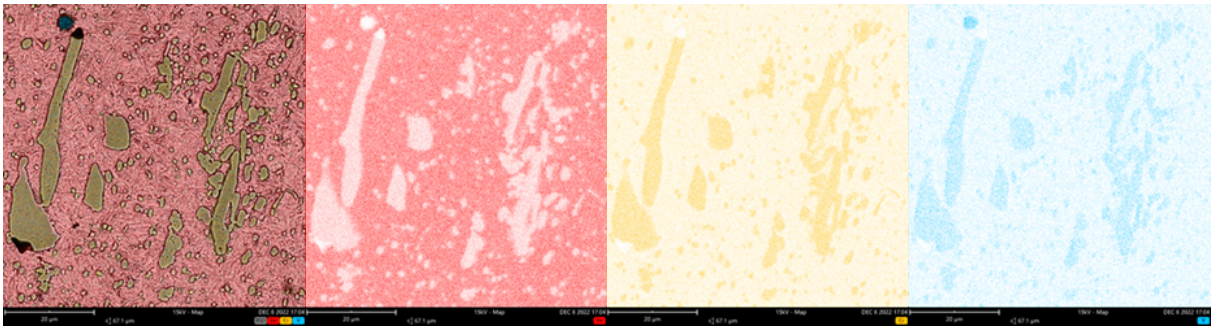
3.4. Microscopic tests after tribological tests

The microscopic examinations were also conducted in the sub-surface area in order to determine the effect of the mechanical operation on the changes in the operational surface layer. For the sub-surface layer of sample 960/450, in the light microscopic image, no significant changes caused by the mechanical operation were observed in the



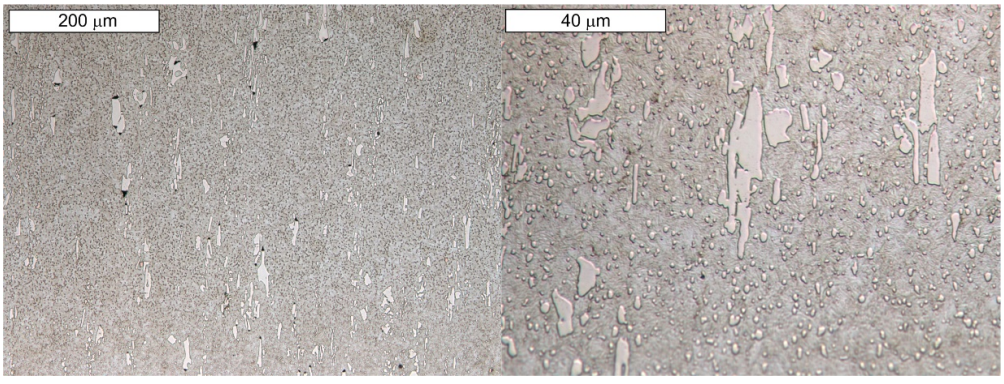
(A) (B)

Fig. 8. View of (A) microstructure of steel NC11. sample 960/450 (B) magnified fragment of the area. Light microscopy, etched state



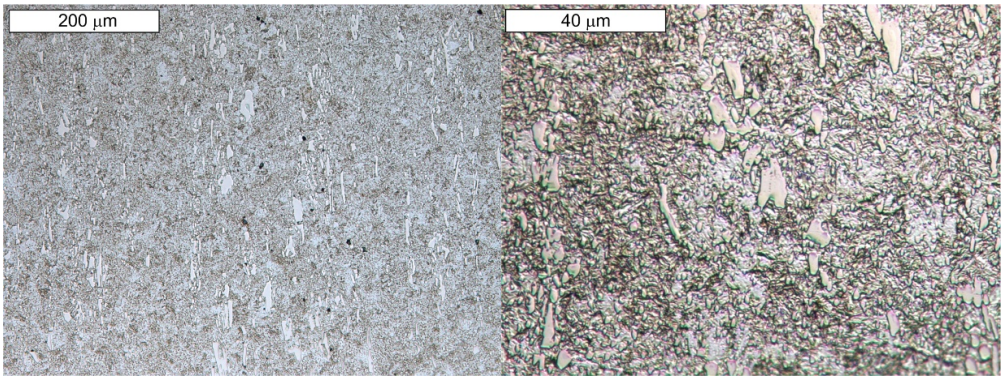
(A) (B) (C) (D)

Fig. 9. Microscopic SEM image, sample 960/450 (A) with the distribution of: iron (B), chromium (C) and vanadium (D). SEM/EDS



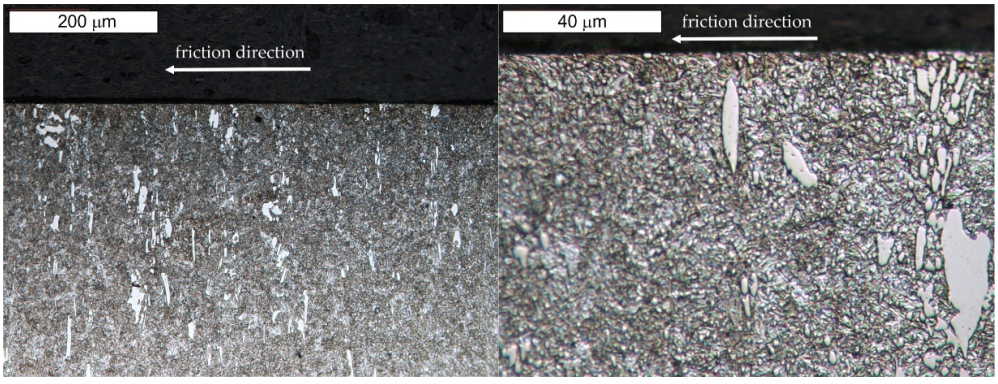
(A) (B)

Fig. 10. View of (A) microstructure of steel NC11LV – sample 1060/450 (B) magnified fragment of the area. Light microscopy, etched state



(A) (B)

Fig. 11. View of (A) microstructure of steel NC11LV – sample 1020/200, (B) magnified, fragment of the area. Light microscopy, etched state



(A) (B)

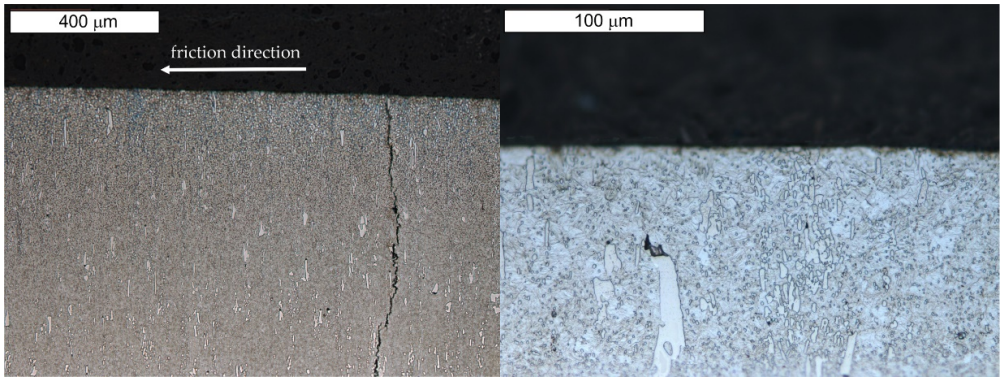
Fig. 12. View of (A) microstructure of steel NC11LV in the sub-surface area in sample 960/450, (B) magnified fragment of the area. Light microscopy, etched state

structure (Figure 12). In the sub-surface area, we can see only slight plastic deformations along the friction direction. The carbide bands in all the tests were arranged perpendicular to the examined surface.

In the case of sample 1060/450, in the sub-surface area, in the microscopic images, it is possible to see the presence of cracks propagating perpendicular to the surface the friction track (Figure 13). They were formed as a result of the mechanical operation resulting from the pressure of the ball (Hertzian stress) constituting a counter-surface in the tribological tests. Cracks were observed only in the area of the friction track.

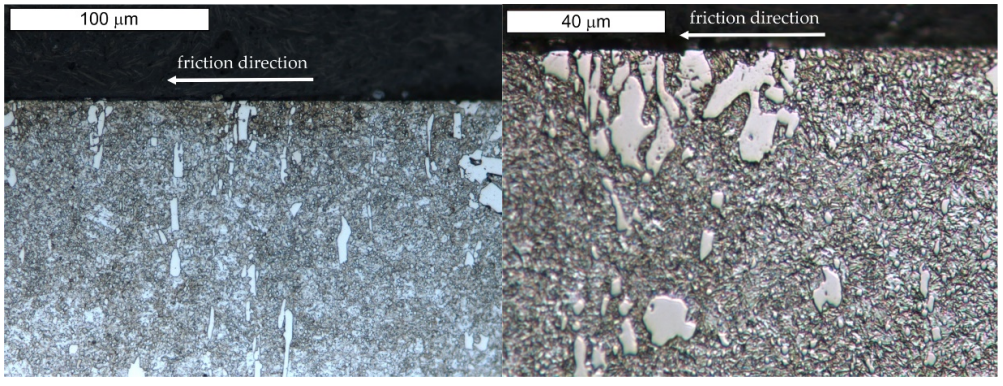
The increased material brittleness is connected with the very high hardness of steel obtained after the heat treatment. In this case, no significant changes were observed (apart from the cracks along the friction track) in the sub-surface area in the light microscopy image. Austenitizing at a higher temperature should result in a higher residual austenite content. However, the retained austenite decomposes during tempering at 450°C. For this reason, the increased hardness of 1060°C-quenched steel should not be associated with the residual austenite content. In addition, its presence should contribute to a reduction in hardness.

In the analysis of the light microscopy images of sample 1020/200 (Figure 14) in the sub-surface area, we can see slight plastic deformations in the



(A) (B)

Fig. 13. View of (A) microscopy of steel NC11LV in the sub-surface area, sample 1060/450, (B) magnified fragment of the area. Light microscopy, etched state



(A) (B)

Fig. 14. View of (A) microstructure of steel NC11LV in the sub-surface area of sample 1020/200, (B) magnified fragment of the area. Light microscopy, etched state

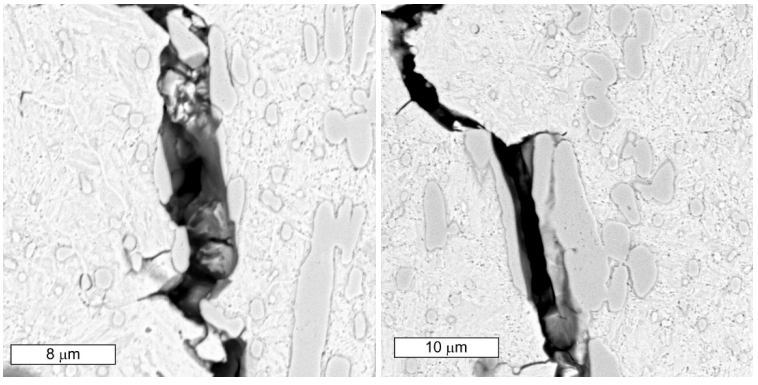


Fig. 15. Course of a crack developing on the surface. Etched state, SEM – sample 1060/450

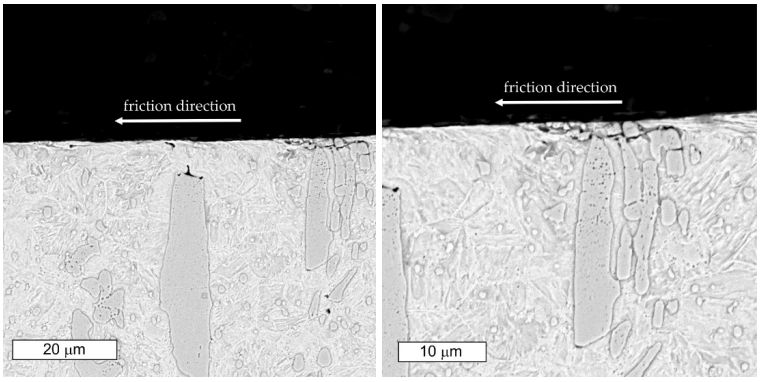


Fig. 16. Spalling of carbides observed in the sub-surface area of steel in state 2. Etched state, SEM, sample 1060/450

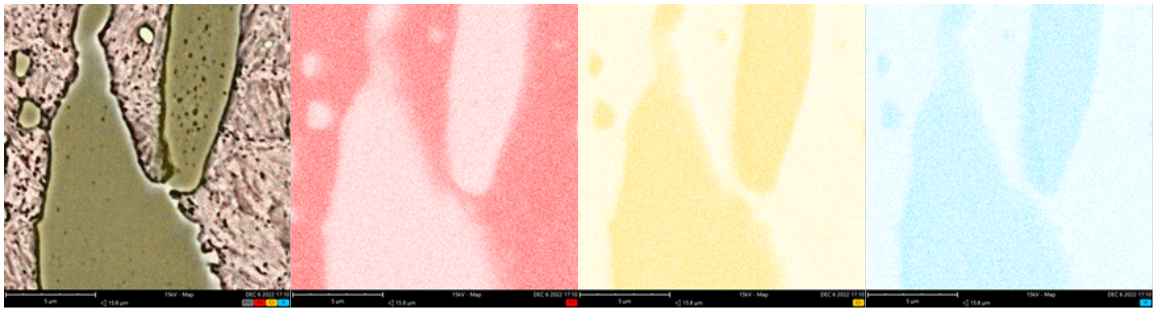
longitudinal direction to that of the friction test. We can observe a local loss of continuity between the carbide precipitates and the matrix, although without macroscopic material decohesion.

The investigations were also extended by an analysis of the sub-surface area with the use of scanning electron microscopy methods. Detailed analyses were performed especially of sample 1060/450, which demonstrated cracks visible in the light microscopy image (Figure 13). For this sample, it was established that the developing crack propagated further within the matrix, but the cracking could also have occurred in the case of the carbide precipitates. The cracks initiated in the matrix propagate further along it. The presence of carbides favors a change in the direction and separation of the developing crack, causing a reduction of the crack propagation speed (Figure 15). When the carbides were within the friction area, the weakened carbides underwent local cracking, which would favor spalling at the further stages. This translates to a higher wear of this sample, despite the clearly higher hardness compared to the other samples. The authors of the study [28] stated that cracks are formed as a result of cooperation of tensile and shear stresses working on the surface, and the crack itself is dependent on their orientation in respect to the abraded surface and the abrasion direction.

The dissolution of carbides in austenite depends on temperature, and the properties of tool steel after hardening are dependent on the amount of the alloy elements dissolved in the austenite. The SEM images obtained from the material austenitized at a higher temperature (sample 1060/450), which proves that the higher austenitization temperature enabled the initiation of dissolution (partial melting) of the carbides contained in the microstructure (Figure 16). This resulted in an increase of the solution strengthening of the formed martensite, which translated to a much higher hardness of the matrix and thus the whole material. A side effect was a simultaneous increase of material brittleness. The increase in brittleness was conducive to easier spalling of the surface during tribological interactions. This ultimately translated into greater wear, despite the higher hardness of the steel under these conditions.

The data in the literature show that a temperature of 1120°C is sufficient for the dissolution of M_7C_3-type carbides. During the heating of steel until tempering, the M_7C_3 carbides are dissolved first, while the thermally more stable M_6C and MC carbides hinder the grain growth. It has been established that, in the case of chromium carbides Cr_7C_3, the melting point is within a range of 900°C to 950°C [29]. Vanadium increases the melting point by about 90°C.

The data in the literature demonstrate that, during prolonged annealing, M_7C_3-type carbides can also undergo transformation into $M_{23}C_6$ carbides by way of diffusion. Wieczerzak et al. [18] stated that the transformation takes place at high temperatures owing to the diffusion of iron into the matrix



(A) (B) (C) (D)

Fig. 17. A microscopic SEM image, sample 1060/450 (A) together with the distribution of: iron (A), chromium (B) and vanadium (D)

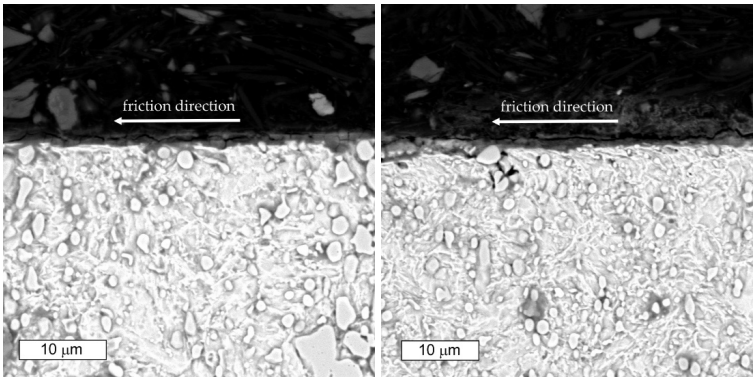


Fig. 18. Surface changes of steel NC11LV. Etched state, SEM – sample 1020/200

and chromium from the matrix to the peripheral regions. This is attributed to the fact that the peripheral regions are closer to the matrix, with the result that the diffusion occurs easier. In consequence, the transformation takes place mostly in the peripheral regions of the M_7C_3 type carbides [30]. In the meantime, Kondrat'ev et al. [17] suggest that the transformation of M_7C_3 into $M_{23}C_6$ begins from the core (the center) of the M_7C_3 carbides. Regardless of the mechanism, however, it has been established that during the 100 h of annealing at 1050°C, a complete transformation of M_7C_3 to $M_{23}C_6$ can take place [31]. The conducted microscopic SEM observations of the sample in state 1060/450 did not show any clear inhomogeneity, which would point to the occurrence of a transformation (Figure 17).

The microscopic SEM analysis performed in the direction transverse to the friction direction of the remaining sample (Figure 18) demonstrated the formation of surface irregularities, which point to the occurrence of the ridging phenomenon.

The visible traces of spallings in the magnified image are the effect of the high hardness of the carbides, whereas the detached fractions are smaller than in the case of samples 960/450 and 1060/450, which can be observed in the measurements of the material loss in the ball-on-disc test.

4. Discussion

The complex performance examinations of tool steel NC11LV in different variants of heat treatment show that the highest abrasion wear resistance based on the ball-on-disc tests is demonstrated by the sample hardened at 1020°C and next tempered at 200°C. In the case of the other heat treatments, it was not possible to reach the set goal, which was

to increase the material's ductility. This justifies a continued application of this heat treatment variant for machine elements in the process of forming ceramic roof tiles, including the tools forming the band. One direction for further research will be verification of the possibility of using other treatment methods to ensure prolonged material durability, such as thermo-chemical treatment or protective coatings. The presence of M_7C_3-type carbides is a factor which translates to high hardness of the examined material. In the case of the application of a high austenitization temperature reaching 1060°C, we can observe partial melting of these carbides in the austenite, which results in an increase of the solution strengthening of the martensite formed and translates to a much higher hardness of the matrix. A side defect was a simultaneous increase of the material's brittleness. In the case of the sample austenitized at 1060°C, the presence of cracks developing perpendicular to the surface was observed; these were formed as a result of the mechanical operation resulting from the pressure of the ball used in the tribological tests. The increased material brittleness is connected with the very high hardness of the steel obtained after this heat treatment. It is interesting that the increases in observed brittleness for this sample did not translate to a clear drop of the already low impact strength. The cracks initiated in the matrix propagated further along it. However, it was observed that cracking could have also occurred in the case of the carbide precipitates.

5. Conclusions

This study performed a comparative analysis of selected variants of heat treatment of tool steel NC11LV. The tests were conducted on the characteristics of abrasive wear resistance in order to investigate the possibility of its application in the process of mass forming in the production of ceramic roof tiles. The analysis supported the following conclusions:

- The lowest wear was demonstrated by the sample with the highest hardness value of 805HV1 (65 HRC), which was obtained after the classic heat treatment. The highest wear was, in turn, exhibited by the sample hardened at 1060°C and then tempered at 450°C.
- At the same time, the hardness tests show that, in all the cases, a higher hardness reduced the abrasive wear. In the investigations conducted, the highest material loss took place for the sample with a hardness of 795 HV1, while the lowest loss occurred in the sample with a hardness of 485 HV1. This was caused by the excessive spalling of the much harder material, which, at the further stages of the ball-on-disc test, constituted an abradant leading to increased wear.
- The impact strength measurements showed that tool steel NC11LV, regardless of the applied heat treatment, is characterized by low ductility. This means that this steel grade should be avoided in applications involving the risk of impact loads. The lowest impact strength was demonstrated by the material after the classic heat treatment; however, the differences determined do not have a clear effect on the material's ductility. No significant influence of a temperature increase on the impact strength value was observed.
- In the case of the steel after the classic heat treatment and after quenching combined with tempering at 450°C, only slight plastic deformations were observed in the sub-surface layer in the longitudinal direction to that of the friction test. The lack of traces of plastic deformation in the sample austenitized at 1060°C only confirms its high brittleness.

Acknowledgements

The research was carried out as part of the implementation doctorate no. DWD/5/0186/202, Poland, "Analysis of exploitation and development of effective methods to increase the durability of tools used in the process of forming a band intended for ceramic roof tiles"

References

[1] Radziszewski P. The steel wheel abrasion test (SWAT): a tool to study wear, friction and ore breakage in the

mining industry. *Wear.* 2009; 267:92–8. https://doi.org/10.1016/j.wear.2009.01.003.

[2] Holmberg K, Kivikytö-Reponen P, Härkisaari P, Valtonen K, Erdemir A. Global energy consumption due to friction and wear in the mining industry. *Tribology International*. 2017; 115:116–39. https://doi.org/10.1016/j.triboint.2017.05.010.

[3] Ligier K, Zemlik M, Lemecha M, Konat Ł, Napiórkowski J. Analysis of wear properties of Hardox steels in different soil conditions. *Materials.* 2022; 15:7622. https://doi.org/10.3390/ma15217622.

[4] Ťavodová M, Vargová M, Krilek J, Stančeková D. Analysis of damaged delimber knives and the possibility of increasing their service life. *Manufacturing Technology.* 2022; 22:80–8. https://doi.org/10.21062/mft.2022.011.

[5] Mirski Z, Fałek Z. Welded containers for scrap and debris transport of 450 Hardox steel. *Przegląd Spawalnictwa* 2015; 87. https://doi.org/10.26628/ps.v87i8.428.

[6] Illera LC, Illera CC, Contreras KA. Raw material for the ceramic industry in Norte de Santander. III. Assessment of the technological properties when the residue test of deep abrasion is added. *Boletín de La Sociedad Española de Cerámica y Vidrio*. 2015; 54:77–83. https://doi.org/10.1016/j.bsecv.2015.03.005.

[7] Händle F. Mixing and kneading: the art of ceramic extrusion. Cham: Springer International Publishing; 2019. p. 49–55. https://doi.org/10.1007/978-3-030-05255-3_7.

[8] Vergnes B. Influence of processing conditions on the preparation of clay-based nanocomposites by twin-screw extrusion. *International Polymer Processing.* 2019; 34:482–501. https://doi.org/10.3139/217.3827.

[9] Wiedmann W, Hölzel M. Twin-screw extruders in ceramic extrusion. In: Händle F, editor. Extrusion in ceramics, Berlin, Heidelberg: Springer Berlin Heidelberg; 2009, p. 241–58. https://doi.org/10.1007/978-3-540-27102-4_13.

[10] Berger H. Dies, pressure heads, strainer plates and more. In: Händle F, editor. Extrusion in ceramics. Berlin, Heidelberg: Springer Berlin Heidelberg; 2009, p. 221–39. https://doi.org/10.1007/978-3-540-27102-4_12.

[11] Marzec J, Hawryluk M, Rychlik M, Lachowicz MM, Suliga M. Preliminary studies of the durability of tools used to form ceramic tiles made of Hardox 600 and NC11LV steel. *Materials.* 2021; 14:1262. https://doi.org/10.3390/ma14051262.

[12] Konat Ł, Jasiński R, Białobrzeska B, Szczepański Ł. Analysis of the static and dynamic properties of wear-resistant Hardox 600 steel in the context of its application in working elements. *Materials Science-Poland*. 2021; 39:86–102. https://doi.org/10.2478/msp-2021-0007.

[13] Berkowski L. Influence of structure on the effects of nitriding chromium ledeburitic steels. Part 1: Information about test materials (in Polish). *Obróbka Plastyczna Metali*. n.d.:2005.

[14] Berkowski L, Borkowski J. The influence of structure of the results of the nitriding of ledeburitic chromium steels. Part III. Heat treatment conditions of NC11LV steel. *Obróbka Plastyczna Metali.* 2007; XVIII:3–12.

[15] Budzyński P, Tarkowski P, Penkała P. Influence of nitrogen ion implantation on tribological properties of tool steel NC10. *Vacuum.* 2001; 63:731–6. https://doi.org/10.1016/S0042-207X(01)00266-4.

[16] Hryniewicz T, Nykiel T. Fluctuations in chemical composition of M-$_7C_3$ carbides in the soft annealed Nc11lv/D2 steel. *Advances in Materials Science.* 2014; 14:24–30. https://doi.org/10.2478/adms-2014-0003.

[17] Kondrat'ev SYu, Kraposhin VS, Anastasiadi GP, Talis AL. Experimental observation and crystallographic description of M_7C_3 carbide transformation in Fe–Cr–Ni–C HP type alloy. *Acta Materialia.* 2015; 100:275–81. https://doi.org/10.1016/j.actamat.2015.08.056.

[18] Wieczerzak K, Bala P, Dziurka R, Tokarski T, Cios G, Koziel T, et al. The effect of temperature on the evolution of eutectic carbides and $M_7C_3 \rightarrow M_{23}C_6$ carbides reaction in the rapidly solidified Fe-Cr-C alloy. *Journal of Alloys and Compounds*. 2017; 698:673–84. https://doi.org/10.1016/j.jallcom.2016.12.252.

[19] Januszewicz B, Wołowiec E, Kula P. The role of carbides in formation of surface layer on steel X153CrMoV12 due to low-pressure nitriding (vacuum nitriding). *Metal Science and Heat Treatment.* 2015; 57:32–5. https://doi.org/10.1007/s11041-015-9830-5.

[20] Berkowski L, Borkowski J. The influence of structure on the results of the nitriding of ledeburitic chromium steels. Part VIII. Investigation of utilization properties of tool materials. *Obróbka Plastyczna Metali*. 2009; XX:3–16.

[21] Hawryluk M, Lachowicz MM, Marzec J, Nowak K, Suliga M. Comparative analysis of the wear of NC11LV and Hardox 600 steel used in tools for extrusion of clay strands in the process of producing ceramic roof tiles. *Materials.* 2022; 16:293. https://doi.org/10.3390/ma16010293.

[22] Rendón J, Olsson M. Abrasive wear resistance of some commercial abrasion resistant steels evaluated by laboratory test methods. *Wear*. 2009; 267:2055–61. https://doi.org/10.1016/j.wear.2009.08.005.

[23] Dohda K, Boher C, Rezai-Aria F, Mahayotsanun N. Tribology in metal forming at elevated temperatures. *Friction*. 2015; 3:1–27. https://doi.org/10.1007/s40544-015-0077-3.

[24] Białobrzeska B. The influence of boron on the resistance to abrasion of quenched low-alloy steels. *Wear.* 2022; 500–501:204345. https://doi.org/10.1016/j.wear.2022.204345.

[25] Bender W. Types of extrusion units. In: Händle F, edi-

tor. Extrusion in ceramics. Berlin, Heidelberg: Springer Berlin Heidelberg; 2009, p. 59–84. https://doi.org/10.1007/978-3-540-27102-4_4.

[26] Albertin E, Sinatora A. Effect of carbide fraction and matrix microstructure on the wear of cast iron balls tested in a laboratory ball mill. *Wear*. 2001; 250:492–501. https://doi.org/10.1016/S0043-1648(01)00664-0.

[27] Wilmes S, Zwick G. Effect of niobium and vanadium as an alloying element in tool steels with high chromium content, Proceedings of the 6th International Tooling Conference: the use of tool steels: experience and research; Karlstad, Sweden, 10 - 13 September 2002

[28] Doğan ÖN, Hawk JA. Effect of carbide orientation on abrasion of high Cr white cast iron. *Wear*. 1995; 189:136–42. https://doi.org/10.1016/0043-1648(95)06682-9.

[29] Cabrol E, Bellot C, Lamesle P, Delagnes D, Povoden-Karadeniz E. Experimental investigation and thermodynamic modeling of molybdenum and vanadium-containing carbide hardened iron-based alloys. *Journal of Alloys and Compounds*. 2013; 556:203–9. https://doi.org/10.1016/j.jallcom.2012.12.119.

[30] Gorunov AI. Investigation of M7C3, M23C6 and M3C carbides synthesized on austenitic stainless steel and carbon fibers using laser metal deposition. *Surface and Coatings Technology*. 2020; 401:126294. https://doi.org/10.1016/j.surfcoat.2020.126294.

[31] Novák P, Nová K, Jaworska L, Shishkin A. Identification of carbides in tool steel by selective etching. *Defect and Diffision Forum*. 2019; 395:55–63. https://doi.org/10.4028/www.scientific.net/DDF.395.55.

Received 2023-04-19
Accepted 2023-06-07